Hydraulic permeability of (un)bounded fibrous media using the lattice Boltzmann method

Clague, D. S.; Kandhai, D.; Zhang, R.; Sloot, Peter M. A.

2000

Clague, D. S., Kandhai, D., Zhang, R., & Sloot, P. M. A. (2000). Hydraulic permeability of (un)bounded fibrous media using the lattice Boltzmann method. Physical Review E, 61(1), 616-625.

https://hdl.handle.net/10356/84483

https://doi.org/10.1103/PhysRevE.61.616

Hydraulic permeability of (un)bounded fibrous media using the lattice Boltzmann method

D. S. Clague*
Center for Nonlinear Studies, MS-B258, Los Alamos National Laboratory, Los Alamos, New Mexico 87545

B. D. Kandhai†
Department of Mathematics, Computer Science, Physics and Astronomy, University of Amsterdam, Kruislaan 403, NL-1098 SJ, Amsterdam, The Netherlands

R. Zhang‡
Center for Nonlinear Studies, MS-B258, Los Alamos National Laboratory, Los Alamos, New Mexico 87545

P. M. A. Sloot§
Department of Mathematics, Computer Science, Physics and Astronomy, University of Amsterdam, Kruislaan 403, NL-1098 SJ, Amsterdam, The Netherlands

(Received 25 February 1999; revised manuscript received 23 September 1999)

Several articles have been written regarding the hydraulic permeability of ordered and disordered fibrous media. Here, we explore wall effects on hydraulic permeabilities for ordered and disordered media using the lattice Boltzmann (LB) simulation method. Simulation results are found to be in excellent agreement with the semi analytic result of Sangani and Acrivos, and simulation results for disordered media are in good agreement with the results of Jackson and James and Higdon and Ford's fcc lattice. The macroscopic behavior, the hydraulic permeability, shows a distinct connection with the geometry of the system. This connection is explored and elucidated for ordered and disordered media. Finally, hydraulic permeabilities for bounded media at various wall separations are presented for both ordered and disordered media and results are compared with hydraulic permeabilities calculated for the unbounded media, and a phenomenological correlation is presented to facilitate rapid prediction of hydraulic permeabilities for both unbounded and bounded fibrous media.

PACS number(s): 47.55.Mh

I. INTRODUCTION

In the study and characterization of fluid flow in fibrous media, the transport property of interest is the hydraulic permeability [4]. Example processes that involve such media include ultra filtration, gel permeation chromatography, and filtration of blood (dialysis). These and other examples typically involve flow through bounded fibrous media, i.e., wall effects. As noted by Tsay and Weinbaum [5] and Lee and Fung [6], the presence of bounding walls can have a profound effect on fluid flow rates. Here we examine wall effects on restricted flow through fibrous media.

The hydraulic permeability of fibrous media has been the subject of many studies [2–4,7,8]. In these studies, a variety of techniques have been employed to probe the behavior of fluid flow in such media. All of these efforts have contributed to understanding the physics of flow in fibrous media. The study of Tsay and Weinbaum [5], however, is unique in that they explore the effects of walls on flow through ordered, biperiodic media made up of cylinders. They develop an analytic expression based on effective medium theory to facilitate rapid predictions of hydraulic permeabilities for bounded fibrous media. In their work, they also note that the critical parameter in such flow systems is the cylinder-cylinder separation rather than fiber volume fraction; see Ref. [5]. In the work presented here, we explore both wall effects and the influence of the cylinder-cylinder spacing on the permeability. For a more complete look at the body of literature in this area, the interested reader is directed to the works of Jackson and James [2], Higdon and Ford [3], Clague and Phillips [4], and Skartsis *et al.* [9].

In the sections to follow, we rigorously benchmark the lattice Boltzmann (LB) method with well-established results for two-dimensional [1] and three-dimensional [3] systems of fibrous media and explore the intuitively obvious connection between the spacing between cylinders in the system and the calculated hydraulic permeabilities. With this foundation, we explore wall effects on the Darcy permeability for ordered and disordered fibrous media for a complete range of solids fractions. Since the effective medium theory is accurate only in the dilute limit, we also put forth a correlation for bounded fibrous media to facilitate more accurate predictions of hydraulic permeabilities for intermediate fiber volume fractions.

The remainder of this paper is broken up into six additional sections. In Sec. II, we briefly present the LB simulation method and show how to use the LB method to calculate hydraulic permeabilities, and in Sec. III, we discuss the fibrous media studied and present formulas to calculate the

*Author to whom correspondence should be directed. Present mailing address: Lawrence Livermore National Laboratory, P.O. Box 808, Mail Stop L-223 Livermore, CA 94550. Electronic address: clague1@llnl.gov

†Electronic address: kandhai@wins.uva.nl

‡Electronic address: raoyang@lanl.gov

§Electronic address: peterslo@wins.uva.nl

half distance between cylinders for each system as a function of fiber volume fraction. Section IV contains a simple scaling estimate for calculating hydraulic permeabilities and comparisons between our LB simulation results and well-accepted results for two- and three-dimensional media. Simulation results and the associated geometry of each system are compared and discussed. In Sec. V, we present calculated hydraulic permeabilities for bounded fibrous media. This includes ordered and disordered media. A phenomenological correlation is presented to provide a rapid estimation of hydraulic permeabilities for moderate fiber volume fractions. Finally, in Sec. VI, we discuss the major conclusions of our findings.

II. THEORETICAL BACKGROUND

In the study of fluid flow through porous media at low Reynolds number, the transport property of interest is the hydraulic permeability, k. The hydraulic permeability is a measure of the fluid conductance in the porous medium [10] and is related to the average fluid velocity and the pressure gradient by Darcy's law [11]

$$\langle \mathbf{v} \rangle = -\frac{\mathbf{K}}{\mu} \cdot \nabla P. \tag{1}$$

Here $\langle \mathbf{v} \rangle$ is the superficial average fluid velocity, μ is the pure fluid viscosity, ∇P is the pressure gradient driving the flow, and $\mathbf{K}$ is the hydraulic permeability tensor. For a homogeneous, isotropic system, $\mathbf{K} = k\boldsymbol{\delta}$, where $\boldsymbol{\delta}$ is the identity tensor. In the work performed here, we use the LB method [12] to calculate k for fibrous media.

A. Lattice Boltzmann method

There are many derivations of the lattice Boltzmann equation and descriptions of the LB method [12–15]. Suffice it to say, we use the LB method to solve two- and three-dimensional hydraulic permeability problems. We use an equispaced square lattice for all systems considered. For the three-dimensional flow systems to be presented in Sec. IV and Sec. V, we use both the 15 and 19 lattice velocity models, and it is found at low Reynolds number flows that both models yielded nearly identical results. Furthermore, to account for solid boundaries, we use the bounce back scheme. As shown by Kandhai *et al.* [16], the simple bounce back scheme achieves better than first-order accuracy when the position of the boundary is taken to be at the halfway position along lattice links that represent the transition from solid to liquid phase [12].

The fluid density and momentum density are calculated in the usual way [12,17], and with the bounce back scheme, we have all of the necessary information to calculate the hydraulic permeability. Based on Eq. (1), the LB representation for k is given by

$$k = v_{ave}\mu/g. \tag{2}$$

Here, v_{ave} is the velocity of the fluid averaged over the entire domain including lattice sites within the particle [17], and g is the applied pressure gradient or gravitational force on the fluid. To make the permeability dimensionless, we divide k by the square of the characteristic length of the obstacle. For a medium of cylinders of equal thickness, the characteristic length is simply the cylinder radius, i.e., a.

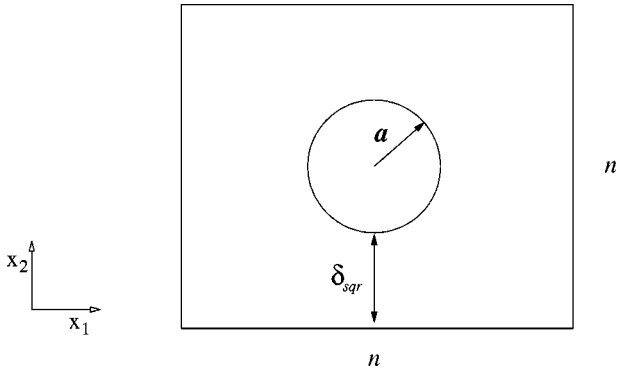

FIG. 1. Two-dimensional simulation cell for a square array of periodic cylinders. The simulation cell consists of a cylinder of radius a centered in a square cell. The simulation cell edge length is n. δ_{sqr} is the distance from the surface of the cylinder to the edge of the cell or the half distance between periodic cylinders.

III. MEDIA STUDIED

The media studied in this work include both two-dimensional and three-dimensional systems. In the case of three-dimensional systems both unbounded and bounded arrays of cylinders are considered. Additionally, the dependence of the hydraulic permeability on the cylinder-cylinder spacing is also examined; consequently, we derive a formula for the half spacing between nearest cylinders for each configuration. This half spacing represents the distance over which the fluid undergoes rapid changes and will be used in the scaling estimate to be presented in Sec. IV.

A. Unbounded media

1. Two-dimensional periodic array of cylinders

To validate simulation results, we compare with the well documented results for the two-dimensional square array of periodic cylinders [1]. For this configuration, the simulation cell simply consists of a circular cylinder of radius a centered in a square fluid domain; see Fig. 1.

This simple simulation cell provides a rigorous test of the LB approach. Also, shown in Fig. 1 is the half spacing δ_{sqr} between neighboring, periodic cylinders. The half spacing for this particular system is related to the fiber volume fraction ϕ by the following expression:

$$\delta_{sqr} = a\left[\frac{1}{2}\left(\frac{\pi}{\phi}\right)^{1/2} - 1\right]. \tag{3}$$

Here, ϕ is the fiber volume fraction of the system.

2. Three-dimensional bcc lattice of cylinders

The bcc lattice provides an additional rigorous test of the LB method for three-dimensional fibrous media. The purposes for looking at the BCC lattice is to perform direct comparisons with Higdon and Ford [3] for a complete range of fiber volume fractions, and to determine the necessary

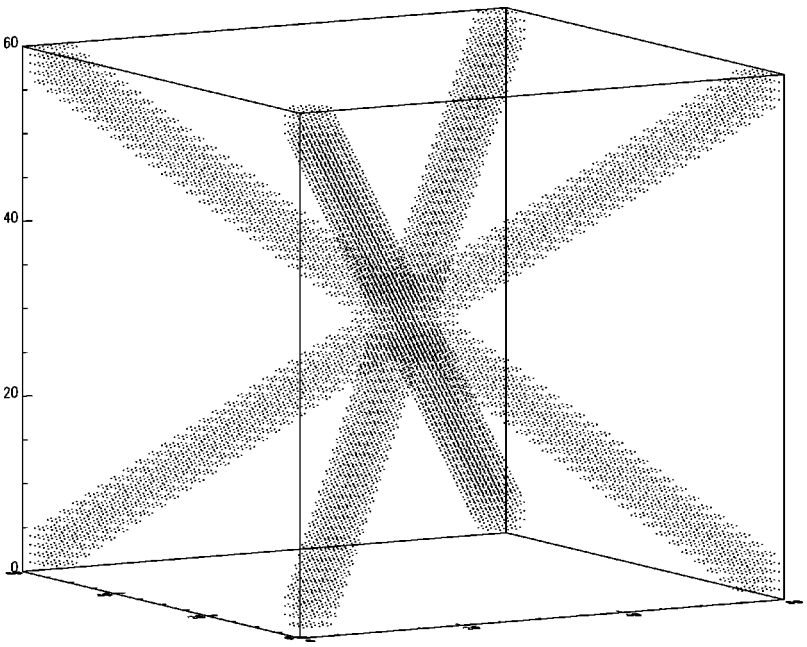

FIG. 2. Three-dimensional, body-centered-cubic (bcc) lattice. The cylinders depicted here have a radius of 3 lattice units. Cylinders emanate from the center of the cell and intersect the eight vertices of the cubic domain. The radius of each of the cylinders is 3 lattice units. The dimensions of the simulation cell are $60\times60\times60$, which represents a fiber volume fraction, $\phi\approx0.36$.

cylinder radii to ensure accurate predictions of hydraulic permeabilities at the higher fiber volume fractions $\phi\geqslant0.5$. Briefly stated, the bcc lattice is simply the body-centered-cubic lattice, and the bcc positions denote locations of fiber-fiber intersections; see Higdon and Ford [3] for details. A LB representation of a typical bcc simulation cell is shown in Fig. 2.

As will be discussed in Sec. IV, the actual cylinder radii to this study this particular cylinder configuration range from 5 to 30 lattice sites or lattice units, but for clarity, the cylinder radius depicted above in Fig. 2 is only three lattice units.

In the bcc system, the fiber volume fraction ϕ is a nonlinear function of the simulation cell edge n [3]. Consequently, the half distance between cylinders, δ_{bcc}, in the dominant flux area is determined here by geometric arguments; see Fig. 3.

Shown in Fig. 3 is the fluid flux area denoted by the inscribed, shaded polygon, in this case a square, which is formed by two adjacent simulation cells. To estimate the half spacing δ_{bcc} between cylinders, we simply take one-half of the square root of this flux area which has been corrected for the finite thickness of the cylinders and divide the resulting characteristic length by 2. The resulting estimate for this particular cylinder-cylinder half spacing is

$$\delta_{bcc}\approx\frac{2^{1/2}}{4}n-a. \tag{4}$$

Here n and a are the same as before; see Fig. 3.

3. Three-dimensional disordered array of cylinders

In the study of disordered fibrous media, we use the approach put forth by Clague and Phillips [18] to generate our media. In their work [18], it was shown that their method does indeed produce statistically random media. For details, the interested reader is directed to their work [18]. There is one subtle difference, however, between the media studied here and that of Clague and Phillips [4,18]. Specifically, in their study, they were not able to allow cylinders to overlap owing to the singular nature of their numerical approach. The lattice Boltzmann method, however, does not exhibit singular behavior when obstacles overlap; consequently, the cylinders here are allowed to freely overlap. For the actual disordered media presented in this work the fiber radii range from 6 to 18 lattice units, and the dimensions of the cubic simulation cells range from 100 to 300 lattice units on an edge depending on fiber volume fraction.

To estimate the mean cylinder-cylinder half spacing for this system, we use Ogston's [19] distribution. Ogston's result gives the distribution of distances to the nearest cylinder in a random medium of infinitely long, freely overlapping cylinders with infinitesimal radii. As a consequence, the overlap volume is zero. Here we modify Ogston's distribution for cylinders of finite radius (see Ref. [20]):

$$\frac{dP}{dD}=\frac{2\phi}{a^2}D\exp\left[-\phi\frac{D^2}{a^2}\right], \tag{5}$$

where P is the probability distribution of distances to the nearest cylinder, and D is the distance.

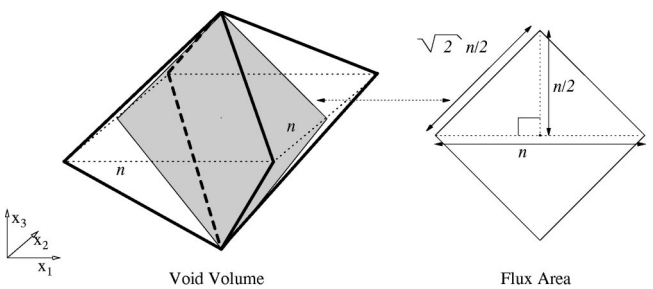

FIG. 3. Void volume formed by two adjacent bcc simulation cells. The bold lines represent the cylinders in the foreground of the system; the bold dashed lines represent the the cylinders in the background. The inscribed shaded region, a square, represents the flux area where the fluid flows. The edge length for an individual, cubic simulation cell is n.

When accounting for cylinders of finite radius, the solid phase volume is double counted at positions of cylinder-cylinder overlap, which skews the distances calculated by Eq. (5). The more the cylinder radius is increased, the greater the error. In the LB method, the solid phase volume is accounted for at precise lattice sites. As a result, the error associated with double counting the overlap volume is known and eliminated; therefore, for the disordered media considered here, we expect the modified version of Ogston's distribution given in Eq. (5) to be valid for all fiber volume fractions considered.

Additionally, Ogston's distribution has the form of a Weibull distribution [21] with known mean and variance. The mean gives the average half distance between adjacent cylinders, or

$$\langle \delta_{ran} \rangle = \frac{a}{\phi^{1/2}} \Gamma\left(\frac{3}{2}\right) - a. \tag{6}$$

Here, $\langle \delta_{ran} \rangle$ is the average half spacing between cylinders, and Γ is the gamma function. The result in Eq. (6) is adjusted for cylinders of finite thickness [19] by subtracting by the cylinder radius a. It also can be shown that $\langle \delta_{ran} \rangle$ is equivalent to δ_{sqr} given in Eq. (3). The difference being the associated standard deviation of $\langle \delta_{ran} \rangle$, which is given by

$$1\sigma = \pm \frac{a}{\phi^{1/2}} \left[\Gamma(2) - \Gamma\left(\frac{3}{2}\right) \right]. \tag{7}$$

The role of this upper bound will be discussed further when the results for disordered media are presented. For example, at maximum packing, $\phi = \pi/4$, the upper bound predicted by Eq. (7) gives a finite cylinder-cylinder spacing of $(a/\pi^{1/2})(2-\pi^{1/2})$. This is a clear indication that fluid flow is possible beyond this critical volume fraction.

B. Bounded media

Here we consider bounded media. Specifically, we examine three-dimensional biperiodic, square, and disordered arrays of cylinders [18]. In each system, the wall-wall separation is specified in terms of the Brinkman screening length [22] α^{-1},

$$\alpha^{-1} = k^{1/2}, \tag{8}$$

where k is the hydraulic permeability of the unbounded rendering of the medium under consideration. The corresponding number n of screening lengths is specified by B, where $B = n\alpha^{-1}$. For the three-dimensional square array of cylinders, the hydraulic permeability used to calculate the desired Brinkman screening lengths is taken from Sangani and Acrivos [1], and for the disordered media, we use the hydraulic permeabilities determined from our LB simulation results for unbounded, disordered media. For both the ordered and disordered media, hydraulic permeabilities are calculated for wall to midplane separations in the range of 2–7 Brinkman screening lengths. The bounded three-dimensional, biperiodic array of cylinders is shown below in Fig. 4.

As shown above, the simulation cell is bounded on top and bottom. Using the notation of Tsay and Weinbaum [5], B is the half distance from a bounding wall to the midplane of the simulation cell, and δ_{sqr}, given by Eq. (3), is again half the distance between neighboring periodic cylinders. The bounded, disordered media include walls in an identical fashion as described in Fig. 4.

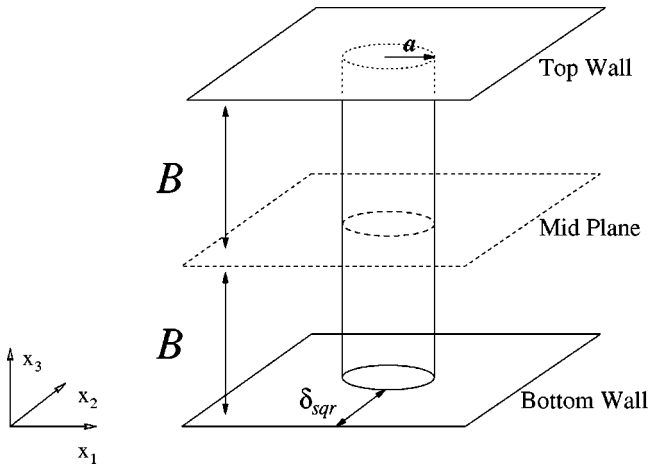

FIG. 4. Three-dimensional, bounded biperiodic simulation cell. The cylinder in the system is bounded on the top and bottom by solid walls. The distance from each wall to the midplane of the simulation cell is B. The half distance between neighboring, periodic cylinders is δ_{sqr} given in Eq. (3).

In Sec. IV to follow, we compare our simulation results with accepted results for a square array of cylinders, the bcc lattice, and a random array of cylinders. We also present the connection between the geometry of the system and the observed macroscopic behavior, k. In Sec. V, we present results for bounded ordered and disordered fibrous media. Additionally, the LB simulation results, unbounded and bounded, are curve fit using a phenomenological model. The fitting parameters are provided to facilitate rapid predications of hydraulic permeabilities of bounded media.

All LB simulations for the square array of cylinders, two and three dimensional, were performed on a single processor Dec Alpha. The mean simulation time was 180 CPU minutes. All three-dimensional disordered media were simulated on the Parsytec CC parallel system in Amsterdam. This includes the three-dimensional bcc lattices and the disordered media. The mean simulation time was 240 CPU minutes. Finally, it should be noted that all fiber volume fractions ϕ are calculated by dividing the total number of solid lattice sites by the total number of lattice sites in the system. The relaxation time τ (see Sec. II) was chosen to be 1 for all simulations. Additionally, the gravitational constant used in Eq. (2) was chosen to ensure that the Reynolds number, based on the particle radius, was much less than 1, $N_{\mathrm{Re}} \sim O(0.0001)$.

IV. RESULTS: UNBOUNDED MEDIA

In this section, we present LB simulation results for flow through unbounded media. Specifically, we calculate the hydraulic permeability for two-dimensional media and for three-dimensional media. We perform resolution studies at the higher volume fractions using the bcc lattice shown in Fig. 2 for comparison with Higdon and Ford [3] over a complete range of fiber volume fractions. Finally, we present

hydraulic permeabilities for disordered media and compare with the cubic lattice model of Jackson and James [2] and Higdon and Ford's [3] result for the fcc lattice, which has been shown to be comparable to random fibrous media [4]. Additionally, we perform a simple scaling analysis based on the system's geometry and compare the predictions from the scaling estimate with the calculated hydraulic permeabilities.

A. Scaling estimate

Before presenting the results, we present here a simple scaling estimate based on an analysis of the governing equations that will be used to explore the connection between the observed hydraulic permeability and the geometry of each system. The following estimate is not intended to be rigorous, but it is intended to simply give physical insight into the geometric dependences of the hydraulic permeabilities to be presented in this section.

The simple scaling analysis is based on the continuity equation

$$\nabla \cdot \mathbf{v} = 0, \tag{9}$$

Stokes equation

$$\mu \nabla^2 \mathbf{v} - \nabla P = 0, \tag{10}$$

and Darcy's law given in Eq. (1). If we take the cylinder-cylinder half spacing for a square array of cylinders as the length scale over which rapid changes in velocity occur, then both x_1 and x_2 scale as δ_{sqr}. From the continuity equation, we obtain a local estimate for v, i.e., $v \sim \langle \mathbf{v} \rangle$, where $\langle \mathbf{v} \rangle$ is the average fluid velocity. In the continuing analysis, we focus on deriving our estimate for the x_2 component of velocity because this is the quantity that represents velocity disturbances orthogonal to the imposed pressure gradient. We now make scaling estimates for the quantities in Stokes equations and find that the left hand side scales as $\mu \langle \mathbf{v} \rangle / \delta_{\mathrm{sqr}}^2$. If we leave the right hand side unchanged as ∇P and make a simple rearrangement of terms, we find that $\langle \mathbf{v} \rangle \sim \delta_{\mathrm{sqr}}^2 / \mu \nabla P$. By directly comparing this estimate with Darcy's law, Eq. (1), we find that

$$k \sim \delta_{sqr}^2 . \tag{11}$$

Here, δ_{sqr} is the half distance between adjacent cylinders in a periodic array of cylinders as described in Sec. III. As will be demonstrated in the sections to follow, this simple estimate for k predicts at what ϕ the hydraulic permeability exhibits interesting behavior and generally captures the expected dependence on ϕ.

B. Two-dimensional periodic array of cylinders

For two-dimensional fibrous media, the result of Sangani and Acrivos [1] is well accepted as the benchmark result for the square array of periodic cylinders. The simulation cell for this configuration is shown in Fig. 1 in Sec. III. Shown in Fig. 5 is our LB results compared to Sangani and Acrivos [1] and the scaling estimate given in Eq. (11). The cylinder radii used in the LB calculations range from 6 to 12 lattice units depending on the fiber volume fraction. As shown, the simulation results exhibit excellent agreement with Sangani and Acrivos [1] over the entire range of fiber volume fractions considered. This result is significant because the LB approach is comparable in the range of ϕ and accuracy to spectral-boundary-element methods used by Higdon and Ford [3].

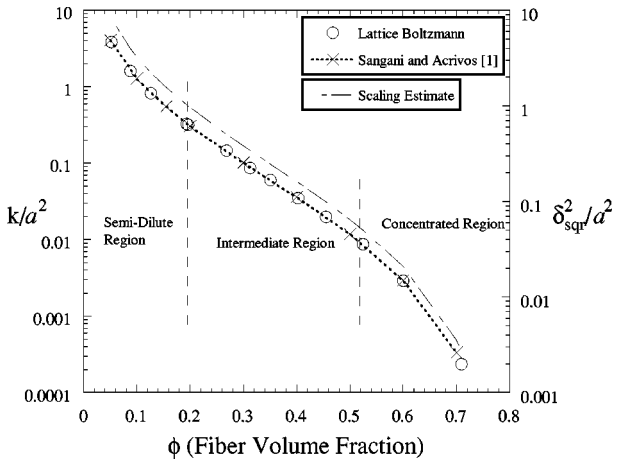

FIG. 5. Hydraulic permeability: two-dimensional square array of periodic cylinders. Nondimensional hydraulic permeabilities calculated using the LB method are compared with the result of Sangani and Acrivos [1], and the scaling estimate given in Eq. (11) for a complete range of fiber volume fractions ϕ. The line through their data is provided to guide the eye. The cylinder radii in the LB simulations range from 6 to 12 lattice units depending on ϕ. The dashed vertical lines separate regions of transitional behavior in the hydraulic permeability. These regions include three distinct ranges of ϕ, i.e., the dilute to semidilute limit, the intermediate range, and the concentrated range. The transitions between these regions occur at $\phi \approx 0.2$ and $\phi \approx 0.52$, respectively.

In Fig. 5, above, there are a few interesting features to be noted. Specifically, in the dilute region $\phi < 0.2$, the hydraulic permeability exhibits the expected [1,2] $-\ln(\phi)/\phi$ dependence on ϕ, and in the intermediate region $0.2 < \phi < 0.5$ the permeability decays in what appears to be an exponential-''like'' fashion [8]. Finally, in the concentrated region $\phi \geqslant 0.5$, where the fluid flux area is significantly reduced, the permeability decreases with the expected, rapid downturn. This behavior occurs in the lubrication-''like'' [1] or percolation limit. It seems intuitively obvious that there is a direct correlation between the observed hydraulic permeability and the available flux area, i.e., the geometric spacing in the medium. As can be clearly seen in Fig. 5, the scaling estimate for k gives the proper trend over the entire range of fiber volume fractions considered and surprisingly predicts permeabilities of the same order of magnitude. Furthermore, the estimate enables us to immediately predict at what ϕ the important regions of behavior are and where interesting transitions in the permeability occur. The more significant result, however, is that the scaling estimate shows that the geometry, i.e., mean spacing between obstacles, of the system is the dominant factor governing the observed permeability.

C. Three-dimensional bcc lattice.

In the study of three-dimensional media, it is important to verify that our LB calculations are indeed correct. Because the interstitial fluid is accounted for at lattice sites, it is necessary to ensure that a minimum of three to five lattice sites

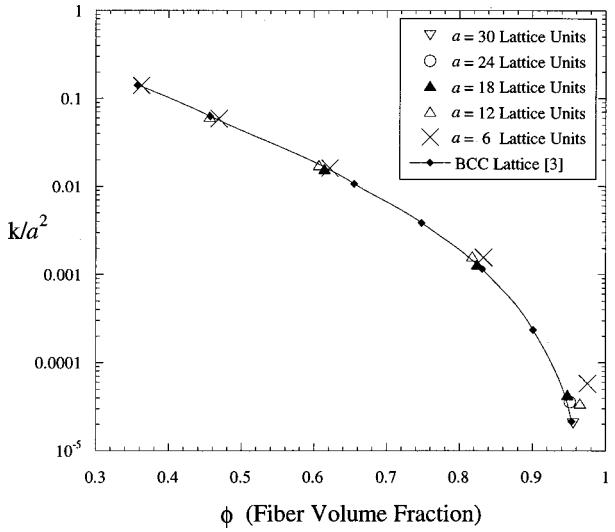

FIG. 6. Resolution study using the bcc lattice. The hydraulic permeability is calculated using the LB method for various cylinder radii a at moderate to high fiber volume fractions $\phi > 0.35$. The results are compared with the results of Higdon and Ford [3] for the same configuration of cylinders. The line through their data is provided to guide the eye.

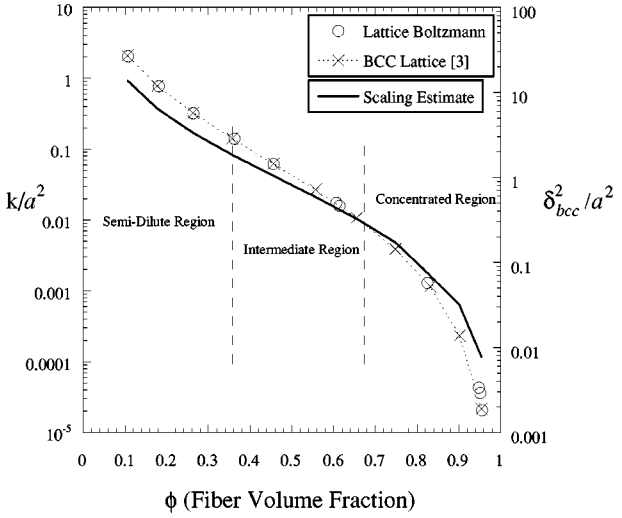

FIG. 7. Hydraulic permeability: bcc lattice of cylinders. Nondimensional hydraulic permeabilities calculated using the LB method are compared with the result of Higdon and Ford [3], and the scaling estimate using Eq. (4) for a periodic, bcc configuration of cylinders or the bcc lattice. The line through their data is provided to guide the eye. The dashed vertical lines separate regions of transitional behavior in the hydraulic permeability. As before, these regions include the dilute to semidilute limit, the intermediate range of ϕ, and the concentrated range. Here the transitions between these regions occur at $\phi \approx 0.35$ and $\phi \approx 0.68$.

exists between solid obstacles to properly capture hydrodynamic interactions. As a consequence, one typically needs to increase both the cylinder radius and the simulation cell proportionately to achieve the desired cylinder-cylinder spacing at a particular fiber volume fraction. To determine the appropriate cylinder radii as a function of fiber volume fraction ϕ, we perform a resolution study and compare with the results of Higdon and Ford [3] for the bcc lattice configuration, see Fig. 2. In their work, Higdon and Ford [3] use spectral-boundary-element methods to calculate the hydraulic permeability. Their approach is both rigorous and accurate for nearly all possible fiber volume fractions. Because the higher fiber volume fractions are the most critical, we perform the study for $\phi \geqslant 0.35$; see Fig. 6 below.

Here we consider cylinder radii ranging from 6 lattice units to 30 lattice units. Results for a cylinder radius of 6 lattice units are accurate up to a fiber volume fraction of 0.6. Using this cylinder radius beyond $\phi = 0.6$ gives a hydraulic permeability greater than expected. To ensure accurate results beyond $\phi = 0.6$, a cylinder radius of 12 lattice units is required to obtain accurate results up to a ϕ of 0.8, and to achieve the accurate results near maximum packing $\phi \approx 0.95$, it is necessary to use a cylinder radius of 18 lattice units.

With this understanding, we can now compare our LB simulation results with the scaling estimate, using Eq. (4) in Eq. (11), and Higdon and Ford's [3] results for the bcc lattice for a complete range of fiber volume fractions; see Fig. 7 below.

As is clearly seen here, the LB results are nearly identical to that of Higdon and Ford [3] over the entire range of fiber volume fractions considered. The shape of the permeability curve exhibits similar regions and transitions as was observed with the square array of cylinders shown above in Fig. 5. Note, also, that for the bcc lattice these regions and the transitions between regions occur at higher fiber volume fractions than for the square array of cylinders. This is due to the fact that in the bcc lattice the fluid flux area is less constrictive than in the square array of cylinders. In particular, the transition between the intermediate range of ϕ and the concentrated region occurs beyond a fiber volume fraction of 0.6 as compared to $\phi \approx 0.5$ for the periodic, square array of cylinders.

Here again the scaling estimate captures the trend and predicts at what fiber volume fractions to expect interesting regions and transitions to occur. The estimate here, however, predicts permeabilities an order of magnitude greater than the LB method, and it also predicts that the rapid downturn begins at $\phi \approx 0.68$ rather than $\phi \approx 0.66$. This is evidence that the estimate for the flux area is not the same as the realized flux area. Given the resolution study and the excellent agreement with Higdon and Ford [3], we can now with confidence calculate hydraulic permeabilities for three-dimensional, disordered fibrous media.

D. Three-dimensional disordered media

We now turn our attention to three-dimensional disordered media. Because we cannot simulate an infinite medium of disordered cylinders, all simulation cells are of sufficient dimensions to ensure that hydrodynamic disturbances generated at the cell edges have little effect on the resulting hydraulic permeability calculations. It has been shown elsewhere [4] that a simulation cell edge length of 14 Brinkman screening lengths is indeed sufficient to eliminate these sources of error. In all of the results to follow, we chose the simulation cell edge length to be a minimum of 14 Brinkman screening lengths, or $n \geqslant 14\alpha^{-1}$. In addition to suppressing edge effects, this also ensures that the cell size is large enough to smooth out local inhomogeneities. For the results

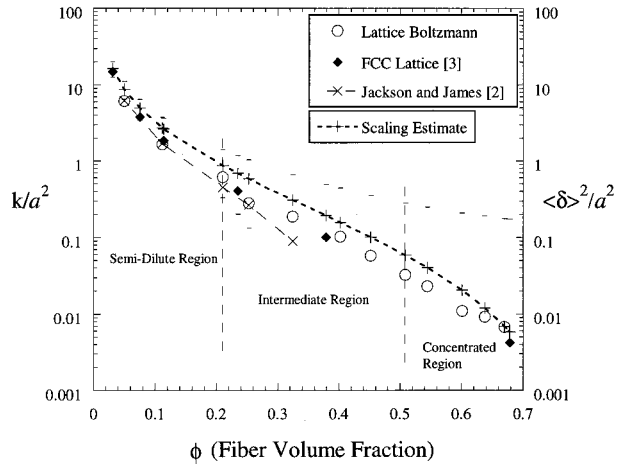

FIG. 8. Hydraulic permeability: three-dimensional, disordered array of cylinders. Nondimensional hydraulic permeabilities for disordered arrays of cylinders are calculated using the LB method. Results are compared with the correlation of Jackson and James [2] [see Eq. (12)], the result of Higdon and Ford [3] for the fcc lattice, and the scaling estimate using Eq. (5). The dashed line through the Jackson- James [2] data is provided to guide the eye. The horizontal lines that bound the scaling estimate represent the $\pm 1\sigma$ given in Eq. (7). The dashed vertical lines identify transitions between regions of dominant behavior. The transition between the dilute to semidilute limit and the intermediate region appears where expected. The expected dramatic down term in permeability between the intermediate and the concentrated regions, however, is not evident at the fiber volume fractions shown.

presented here the ratio n/a is always greater than 18, consistent with the findings above for the bcc lattice; we use cylinder radii, of 6 and 12 lattices units.

In Fig. 8, we compare hydraulic permeabilities calculated using the LB method with the cubic lattice model of Jackson and James [2], which is given by

$$\frac{k}{a^2} = \frac{3}{20\phi}[-\ln(\phi) - 0.931], \tag{12}$$

the fcc lattice result of Higdon and Ford [3], and the scaling estimate, using Eq. (6) in Eq. (13). The cubic lattice model of Jackson and James [2] is only accurate in the dilute limit, i.e., $\phi \leqslant 0.25$, where to leading order the functionality for k/a^2 is $-\ln(\phi)\phi$. This dependence on ϕ in the very dilute limit $\phi \leqslant 0.1$ is well known and accepted. As noted in Fig. 8, our LB result at $\phi = 0.05$ is nearly identical to Jackson and James [2], which is a very promising result; moreover, a curve fit of our simulation data in this domain using the $-\ln(\phi)/\phi$ functionality yields a correlation coefficient of 1, $R = 1$.

We also compare with the results of Higdon and Ford [3] for the fcc lattice. This configuration of cylinders was chosen because it is the best representation of disordered media presented in their work. Our results in the semidilute and concentrated regions exhibit good agreement with Higdon and Ford [3]. Beyond $\phi \geqslant 0.25$, our results predict slightly higher hydraulic permeabilities than Higdon and Ford [3]. This was also the case in the study of flow through a flexible, random mat, performed by Koponen *et al.* [8]. This observed behavior has two plausible explanations. First, in a random or disordered medium, the cylinders sample many more orientations relative to the incident flow field than the fcc lattice; therefore, it is possible to have a higher percentage of cylinders oriented parallel to the flow than in the fcc configuration. Second, while the media are indeed random [18], the probability of the presence of large interstices and or paths that span the finite simulation cell length is increased as the simulation cell size n is reduced. In general, however, the agreement is good, and the LB method provides good results for a wide range of fiber volume fractions.

Also shown is the scaling estimate. The horizontal lines that bound the scaling estimate represent $\pm 1\sigma$. Beyond a fiber volume fraction of 0.3, the lower error bound is such a small value that it does not appear on the logarithmic scale. It should be noted here that the scaling estimate is for local cylinder-cylinder half spacing. In random or disordered media, a chain of these interstices must exist across the entire simulation cell to permit fluid conductance. Given the average half spacing between cylinders, $\langle \delta_{ran} \rangle$, it is a reasonable to assume that this spacing is indeed representative of the average ''channel'' width that spans the medium. The first feature to note here is that the scaling estimate captures the trend and surprisingly estimates permeabilities of the proper order of magnitude. Also, in the semidilute limit the scaling estimate predicts permeabilities similar to the expected $-\ln(\phi)/\phi$ dependence. As noted above, the LB result does not exhibit a downturn consistent with the onset of the percolation limit beyond $\phi \geqslant 0.5$. Considering the upper bound for $\langle \delta_{ran} \rangle, +1\sigma$, it is clear that there exists the probability that the cylinder-cylinder half spacing is large enough, even at the higher fiber volume fractions, so that the expected downturn is not observed. An additional LB simulation was conducted at $\phi = 0.8$ with a cylinder radius of 18 lattice units and an edge length n equal to 300 lattice units. At this fiber volume fraction, the system was found to be percolated. This clearly represents the distinct downturn that we seek (data not shown).

V. RESULTS: BOUNDED MEDIA

Here we present hydraulic permeabilities calculated using the LB method for bounded fibrous media. Results are compared with the appropriate unbounded rendering of the same cylinder configuration. This includes both ordered and disordered media. The LB results are fit with a phenomenological correlation that is based on the scaling estimate given in Eq. (3), existing theory [5,6], and a stretched exponential dependence on ϕ. The fitting parameters are given in tabular form to facilitate use of the result.

A. Bounded, three-dimensional, square array of cylinders

In this subsection, we present LB simulation results for hydraulic permeabilities of bounded ordered media. The simulation cell for the biperiodic, square array of cylinders is shown in Fig. 4. Results for wall to midplane separations ranging from 2 to 7 Brinkman screening lengths α^{-1} are compared with the unbounded result of Sangani and Acrivos [1] in Fig. 9.

The characteristics of the hydraulic permeability curves for each case are similar. The trends exhibit the same transi-

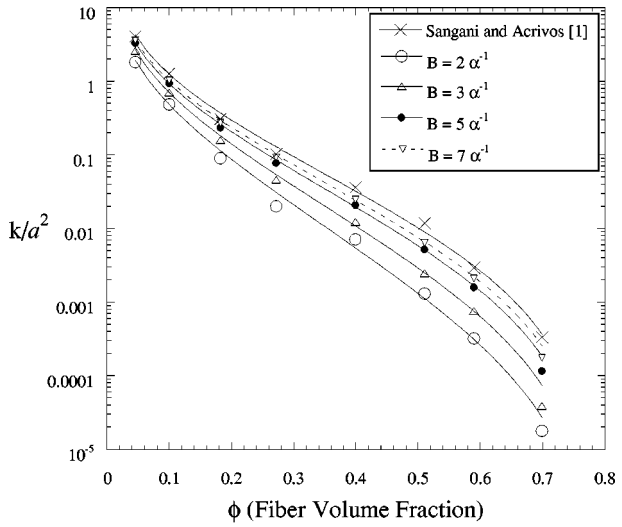

FIG. 9. Hydraulic permeability: bounded three-dimensional, square array of cylinders. Hydraulic permeabilities calculated using the LB method are compared with the unbounded result of Sangani and Acrivos [1] for bounded systems. The wall to midplane separations B considered are 2, 3, 5, and 7 Brinkman screening lengths. Hydraulic permeabilities are made dimensionless with the cylinder radius squared. Here, the lines through the data are from a curve fitting using Eq. (14). The curve-fit parameters are given in Table I.

tions between regions of dominant functional behavior (see Sec. IV) at similar fiber volume fractions. Additionally, the slopes of the curves in regions of dominant functional behavior appear to be similar. The gap between walls, $2B$, causes a noticeable reduction in k over the entire range of fiber volume fractions. The percent differences between the calculated hydraulic permeabilities and the unbounded result are 80%, 66%, 47%, and 38% on average for 2, 3, 5, and 7 Brinkman screening lengths, respectively. These percent differences decrease in an exponential fashion with increasing B. This is consistent with the notion that the bounding walls behave like an effective medium where the gap between the walls represents the average spacing between fixed obstacles.

The line fit through the data comes from a phenomenological model that is based on the scaling estimate in Eq. (11), the effective medium result of Tsay and Weinbaum [5], and a stretched exponential dependence on ϕ to adjust the trend predicted by the scaling estimate for a wider range of fiber volume fractions. In brief, the effective medium result derived by Tsay and Weinbaum [5] is given by

$$k_{bounded}=k\left(1-\frac{\tanh(B/\alpha^{-1})}{B/\alpha^{-1}}\right), \tag{13}$$

where k is the hydraulic permeability of the unbounded rendering of the same medium. As stated by Fu *et al.* [23], the expression given above in Eq. (13) is accurate when the aspect ratio B/a is greater than 5 or when the bounding walls are reasonably far apart. Furthermore, at intermediate and concentrated, $\phi>0.20$, fiber volume fractions the expression given in Eq. (13) captures the correct trend but over predicts hydraulic permeabilities.

By combining Eq. (13) with the appropriate scaling estimate, Eq. (3), and a stretched exponential dependence on ϕ, or $b_1\exp(b_2\phi)$, we arrive at the following curve fit equation used in Fig. 9:

$$k^*_{bounded}=\delta^2_{sqr}[b_1\exp(b_2\phi)]\left(1-\frac{\tanh(B/\alpha^{-1})}{B/\alpha^{-1}}\right), \tag{14}$$

where b_1 and b_2 are the curve fitting parameters. The fitting parameter b_1 rescales the estimated permeability given by δ^2_{sqr}, and b_2 adjusts the slope of the prediction for intermediate to high ϕ. The effective medium approximation in Eq. (13) is merely a constant for a fixed B/α^{-1} (or B') and can be lumped with the constant b_1. Here we distinguish our, curve-fit, estimate for the hydraulic permeability from the effective medium result, Eq. (13), of Tsay and Weinbaum [5] with an asterisk, *.

As shown in Fig. 9, all curve fits exhibit excellent agreement out to a ϕ equal to approximately 0.65. The resulting set of fitting parameters b_1 and b_2 for the wall separations B cited above are given in Table I.

For the fit of the permeabilities of the unbounded media, $B=\infty$, the effective medium term in parentheses is neglected. If we further fit the curve-fit parameters b_1 and b_2 for the bounded results as a function of B with a second-degree polynomial plus a natural logarithmic dependence, i.e., $C_1+C_2B+C_3B^2+C_4\ln(B)$. The resulting coefficients $C_1,\ldots,C_4$ are given below in Table II. The curve-fit equation for b_1 and b_2 nearly matches the data exactly and has a correlation coefficient R of 1. We note, however, that the equation chosen to fit the fitting parameters has no apparent physical meaning. This result is simply provided to enable rapid use of the curve-fit equation given in Eq. (14). All that is necessary to predict hydraulic permeabilities for bounded ordered, fibrous media is knowing the half spacing between adjacent cylinders as a function of fiber volume fraction ϕ and the wall to midplane separation B in terms of Brinkman screening lengths α^{-1}.

TABLE I. Curve-fit parameters, Eq. (14), b_1 and b_2 as a function of the wall to midplane separation, $B(\alpha^{-1})$, for biperiodic, square arrays of cylinders.

B	b_1	b_2
2	0.4369	−4.7912
3	0.4575	−3.8270
5	0.4692	−2.9423
7	0.4705	−2.5775
∞	0.50941	−1.8042

TABLE II. Curve-fit of the ''curve fitting parameters'' in Eq. (14) as a function of the wall to midplane separation, $B(\alpha^{-1})$, for biperiodic, square array of cylinders.

	C_1	C_2	C_3	C_4
b_1	0.4204	−0.0403	0.0016	0.1310
b_2	−6.0877	−0.8671	0.0289	4.1965

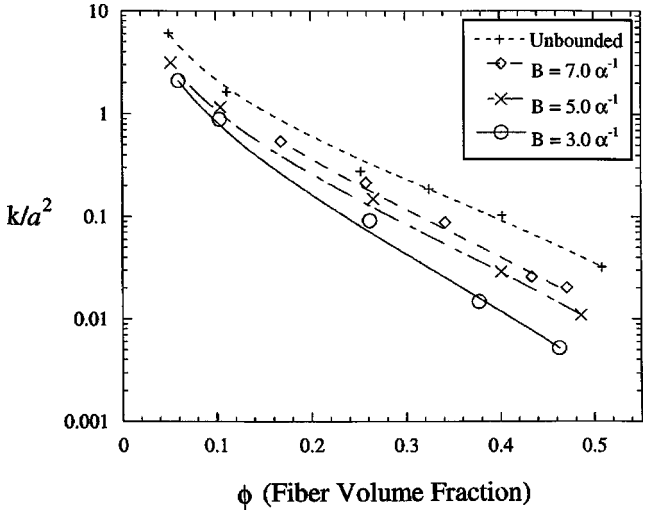

FIG. 10. Hydraulic permeability: bounded three-dimensional, disordered array of cylinders. Hydraulic permeabilities calculated using the LB method for bounded, disordered arrays of cylinders are compared with the unbounded results for the same system presented in Sec. IV. The wall to midplane separations B considered are 3, 5, and 7 Brinkman screening lengths. Hydraulic permeabilities are made dimensionless with the cylinder radius squared. The lines through the data are from a curve fitting using Eq. (14). The curve-fit parameters are given in Table III.

B. Bounded disordered media

Here we calculate hydraulic permeabilities for bounded, disordered fibrous media using the LB method. Again, we compare our LB results for wall to mid-plane separations of 3, 5, and 7 Brinkman screening lengths with results from Sec. IV for the same unbounded configuration of cylinders in Fig. 10.

At these wall to midplane separations the bounding walls have a significant influence on the observed hydraulic permeability; e.g., for $B=5\alpha^{-1}$ at $\phi=0.2$, there is a 61% difference between the calculated hydraulic permeability and the unbounded result. At higher volume fractions $\phi>0.2$, the percent difference relative to the unbounded result is $\approx 75\%$ on average. Also, unlike the ordered media, the slopes in the trends for increasing ϕ steepen as B is reduced below 4 Brinkman screening lengths, and the transition between the dilute and the intermediate regions for each case occurs at $\phi\approx 0.2$.

The apparent difference in the trends and data scatter between the calculated hydraulic permeabilities in Fig. 10 and the ordered results above in Fig. 9 is due in large part to large variations in local fiber volume fractions within the simulation cell, i.e., the ratio of vertical cell edge length n to cylinder radius, n/a, is less than the tolerance, $n/a>12$, necessary for accurate predictions of hydraulic permeabilities; see discussion in Sec. IV. As the simulation cell size is reduced, which is the case when considering bounded, disordered media, local heterogeneities in the microstructure are accentuated. These heterogeneities have a more and more dominant influence on k as the bounding walls are brought closer together. As a result, there is a noticeable increase in variations in the calculated hydraulic permeabilities shown above for $B<\alpha^{-1}$.

TABLE III. Curve-fit parameters, Eq. (14), b_1 and b_2 as a function of the wall to midplane separation, $B(\alpha^{-1})$, for bounded, disordered arrays of cylinders.

B	b_1	b_2
3	0.5977	−4.1839
5	0.5249	−2.6794
7	0.6355	−1.6834
∞	0.71407	−0.51854

Here again the lines through the data obtain from the LB method are a result of curve fits using the appropriate scaling estimate, $\langle \delta_{ran} \rangle$ in Eq. (14) The curve fits capture the expected trends and the important transitions. Also, since we consider a reduced range of ϕ here, the fits are in excellent agreement with the LB result over the majority of the range of fiber volume fractions considered. The curve fitting parameters b_1 and b_2 used in Eq. (14) for the range of wall to midplane separations considered, i.e., for $B=3,5,7$, and ∞, are given in Table III.

Again, for the unbounded system, i.e., for $B=\infty$, the effective medium term in parentheses has been neglected.

As in the case of the bounded ordered system, the fitting parameters for the bounded data are fit to enable rapid predictions of bounded hydraulic permeabilities. The curve-fit function used here to fit the fitting parameters for disordered media is the same as in Sec. (V A). As stated before, this functionality has no apparent physical meaning but is presented to facilitate rapid predictions of hydraulic permeabilities of bounded, disordered media. The curve-fit parameters $C_1, \ldots, C_4$ for b_1 and b_2 as a function of B are given in Table IV.

VI. CONCLUSIONS

In this paper, we have shown that the lattice Boltzmann method is an accurate and versatile method for the study of fluid flow in fibrous media. Hydraulic permeabilities calculated using the LB method for both two- and three-dimensional configurations of unbounded cylinders are in excellent agreement with existing theory [1] and well-established numerical results [3]. Resolution studies using the three-dimensional, bcc lattice in Sec. IV show that LB simulations require greater than three lattice sites between obstacles to properly capture hydrodynamic interactions for stationary media. When applied properly, the LB method is comparable in the range of ϕ and accuracy to boundary element methods [3] in the study of fluid flow through fibrous media. With these foundational results and the ease of including bounding walls in the LB method, this approach readily enables the calculation of hydraulic permeabilities for

TABLE IV. A fit of the curve-fit parameters in Eq. (14) as a function of the wall to midplane separation, $B(\alpha^{-1})$, for bounded, disordered arrays of cylinders.

	C_1	C_2	C_3	C_4
b_1	0.4211	−0.0046	0.0	0.1246
b_2	−7.8261	−0.2350	0.0	4.0000

bounded fibrous media, which previously have required an significant amount of effort [5].

The simple scaling estimate put forth in Sec. IV clearly shows that the geometry of the system is the dominant factor that influences the behavior of the resulting hydraulic permeability. The scaling estimate also enables rapid determination of the trend and important transitions observed in the hydraulic permeability as a function of fiber volume fraction ϕ.

Because the LB method accounts for the solid phase at specific lattice sites, the overlap volume in a three-dimensional, random medium of freely overlapping cylinders of finite radius is known and accounted for appropriately. As a consequence, the modified version of Ogston's distribution [19,20] is considered valid over the entire range of fiber volume fractions studied. Furthermore, the statistical error [see Eq. (7)] predicted by Ogston's distribution demonstrates that in the upper bound, $+1\sigma$, for the average spacing between cylinders does indeed permit sufficient fluid flow so that the onset of the dramatic reduction in permeability predicted by Eq. (6) in the range of ϕ studied was not observed.

The hydraulic permeabilities for unbounded and bounded media calculated using the LB method were curve fit with a phenomenological equation, Eq. (14), to permit rapid calculation of the hydraulic permeabilities of unbounded and bounded fibrous media for a wide range of ϕ. This range includes the semidilute to intermediate fiber volume fractions, i.e., $0.05 \leqslant \phi < 0.7$. The fitting equation is based on the appropriate scaling estimate, Sec. IV, the effective medium estimate put forth by Tsay and Weinbaum [5], and a stretched exponential dependence on ϕ. The curve fit parameters in Eq. (14), b_1 and b_2, have been tabulated in Tables I and III; furthermore, these fit parameters have also been curve fit to enable a rapid prediction of permeabilities for systems with wall to midplane separations not considered here.

[1] A.S. Sangani and A. Acrivos, Int. J. Multiphase Flow **8**, 193 (1982).
[2] G.W. Jackson and D.F. James, Can. J. Chem. Eng. **64**, 364 (1986).
[3] J.J.L. Higdon and G.D. Ford, J. Fluid Mech. **308**, 341 (1996).
[4] D.S. Clague and R.J. Phillips, Phys. Fluids **9**, 1562 (1997).
[5] R. Tsay and S. Weinbaum, J. Fluid Mech. **226**, 125 (1991).
[6] J.S. Lee and Y.C. Fung, J. Fluid Mech. **37**, 657 (1969).
[7] E. Schweers and F. Loffler, Powder Technol. **80**, 191 (1994).
[8] A. Koponen, D. Kandhai, E. Hellen, M. Alava, A. Hoekstra, M. Kataja, K. Niskanen, P. Sloot, and J. Timonen, Phys. Rev. Lett. **80**, 716 (1998).
[9] L. Skartsis, J.L. Kardos, and B. Khomami, Polym. Eng. Sci. **32**, 221 (1992).
[10] D.A. Edwards, M. Shapiro, P. Bar-Yoseph, and M. Shapira, Phys. Fluids A **2**, 45 (1990).
[11] S. Whitaker, Trans. Porous Media **1**, 3 (1986).
[12] Anthony J.C. Ladd, J. Fluid Mech. **271**, 285 (1994).
[13] S. Chen and G.D. Doolen, Annu. Rev. Fluid Mech. **30**, 329 (1998).
[14] X. He and L. Luo, Phys. Rev. E **55**, R6333 (1997).
[15] T. Abe, J. Comput. Phys. **131**, 241 (1997).
[16] B.D. Kandhai, A. Koponen, A. Hoekstra, M. Kataja, J. Timonen, and P.M.A. Sloot, J. Comput. Phys. **150**, 482 (1999).
[17] Anthony J.C. Ladd, J. Fluid Mech. **271**, 311 (1994).
[18] D.S. Clague and R.J. Phillips, Phys. Fluids **8**, 1720 (1996).
[19] A.G. Ogston, Trans. Faraday Soc. **54**, 1754 (1958).
[20] T.F. Kosar and R.J. Phillips, AIChE. J. **41**, 701 (1994).
[21] S. B. Vardeman, *Statistics for Engineering Problem Solving* (PWS, Boston, 1994).
[22] H.C. Brinkman, Appl. Sci. Res., Sect. A **1**, 27 (1947).
[23] B.M. Fu, S. Weinbaum, R.Y. Tsay, and F.E. Curry, J. Biomech. Eng. Trans. ASME, Ser. C: J. Heat Transfer **116**, 502 (1994).